Critical behavior of the spin density wave transition in underdoped $Ba(Fe_{1-x}Co_x)_2As_2$ ($x \leqslant 0.05$): ^{75}As NMR investigation

F. L. Ning,[1,*] M. Fu,[2] D. A. Torchetti,[2] T. Imai,[2,3] A. S. Sefat,[4] P. Cheng,[5] B. Shen,[5] and H.-H. Wen[3,5,6]

[1]*Department of Physics, Zhejiang University, Hangzhou 310027, P. R. China*

[2]*Department of Physics and Astronomy, McMaster University, Hamilton, Ontario, Canada L8S4M1*

[3]*Canadian Institute for Advanced Research, Toronto, Ontario, Canada M5G1Z8*

[4]*Materials Science and Technology Division, Oak Ridge National Laboratory, Tennessee 37831, USA*

[5]*National Laboratory for Superconductivity, Institute of Physics and Beijing National Laboratory for Condensed Matter Physics, Chinese Academy of Sciences, Beijing 100190, P. R. China*

[6]*Center for Superconducting Physics and Materials, National Laboratory for Solid State Microstructures, Department of Physics, Nanjing University, Nanjing 210093, P. R. China*

(Received 4 April 2014; revised manuscript received 20 May 2014; published 25 June 2014)

We investigate the nature of the SDW (spin density wave) transition in the underdoped regime of an iron-based high-T_c superconductor $Ba(Fe_{1-x}Co_x)_2As_2$ by ^{75}As NMR, with primary focus on a composition with $x = 0.02$ ($T_{SDW} = 99$ K). We demonstrate that critical slowing down toward the three-dimensional SDW transition sets in at the tetragonal to orthorhombic structural phase transition $T_s = 105$ K, suggesting strong interplay between structural distortion and spin correlations. In the critical regime between T_s and T_{SDW}, the dynamical structure factor of electron spins $S(\mathbf{q},\omega_n)$ measured with the longitudinal NMR relaxation rate $1/T_1$ exhibits a divergent behavior obeying a power law $1/T_1 \propto \Sigma_{\mathbf{q}} S(\mathbf{q},\omega_n) \sim (T/T_{SDW} - 1)^{-\delta}$ with the critical exponent $\delta \sim 0.33$.

DOI: 10.1103/PhysRevB.89.214511 PACS number(s): 74.70.Xa, 76.60.−k

I. INTRODUCTION

The discovery of superconductivity with T_c as high as 28 ∼ 55 K in iron pnictides [1–5] has regenerated strong interest in the research of high-temperature superconductivity. The parent compound of the so-called 122 ferropnictides, $BaFe_2As_2$, is a semimetallic antiferromagnet; upon cooling, $BaFe_2As_2$ undergoes a first-order spin density wave (SDW) transition at $T_{SDW} \sim 135$ K, accompanied by a tetragonal to orthorhombic structural phase transition at $T_s (= T_{SDW})$ [4,6–8]. Doping a few percent of Co into the Fe sites of $BaFe_2As_2$ quickly suppresses T_{SDW} [9,10] as well as T_s [11], as summarized in Fig. 1. In the lightly Co-doped regime, the structural phase transition takes place first upon cooling, followed by the SDW transition in the orthorhombic phase [11,12]. Superconductivity with optimized $T_c \sim 25$ K appears when T_s and T_{SDW} are completely suppressed by 6% ∼ 8% Co doping [5,9–14]. The nature and origin of the SDW ordering, and its potential relation to the superconducting mechanism, are the subject of intense debates [15].

In this work, we investigate the critical behavior of the SDW transition and its interplay with the structural transition in lightly Co-doped single crystals of $Ba(Fe_{1-x}Co_x)_2As_2$ with $x = 0.02$, 0.04, and 0.05 based on ^{75}As NMR measurements. We will place our primary focus on a composition with $x = 0.02$; thanks to their relatively sharp NMR lines, experimental characterizations of structural and SDW phase transitions are straightforward for this composition. We demonstrate that the structural transition at $T_s = 105$ K triggers the critical slowing down of spin dynamics toward the three-dimensional SDW transition at $T_{SDW} = 99$ K. We found that the critical exponent for the divergence of the dynamical structure factor of electron spins $S(\mathbf{q},\omega_n)$ near the SDW transition is different from $\delta = \frac{1}{2}$ often attributed to itinerant electron magnetism, such as metallic Cr [16]. Instead, we found $\delta \sim 0.33$. This value is nearly identical with the case of a Mott insulator CuO with $\delta = 0.33 \pm 0.01$ [17], and is in reasonable agreement with the theoretically predicted value of $\delta = \nu/2 \sim 0.35$ for insulating three-dimensional (3D) Heisenberg antiferromagnets [18–21]. Here, $\nu \sim 0.7$ is the critical exponent for the spin-spin correlation length ξ, and $\xi \sim (T/T_{SDW} - 1)^{-\nu}$. We also demonstrate that Co doping enhances the density of states $D(E_F)$ of the reconstructed Fermi surfaces below T_{SDW} roughly in proportion to x, based on the enhancement of $1/T_1T$ at low temperatures.

The rest of this paper is organized as follows. In Sec. II, we will briefly describe experimental procedures. In Sec. III, we will discuss our results in the paramagnetic state above T_{SDW}, followed by brief discussions about the SDW ordered state. We will conclude in Sec. IV.

II. EXPERIMENTAL METHODS

We grew single crystals of $Ba(Fe_{1-x}Co_x)_2As_2$ from FeAs flux [5,14]. We carried out NMR measurements using the standard pulsed NMR techniques. For $x = 0.02$, we cleaved a small piece of shiny crystal from a much larger boule used for our previous report [22]. The total mass of the smaller crystal used for this work is about ∼7 mg. It was necessary to use the smaller piece to ensure high homogeneity of the sample. In fact, we found no evidence for a stretched recovery of T_1 [23] in our small homogeneous crystal of $x = 0.02$, contrary to an earlier report that an $x = 0.022$ crystal [24] and lightly doped $LaFeAsO_{1-x}F_x$ crystals [25] exhibit a large distribution of T_1, which implies a large distribution of T_{SDW}. From the sharpness of the divergent behavior of $1/T_1$ and the NMR linewidth, we estimate the upper bound of the distribution of T_s and T_{SDW} as little as ∼0.5 K in our small $x = 0.02$ crystal. Moreover,

*ningfl@zju.edu.cn

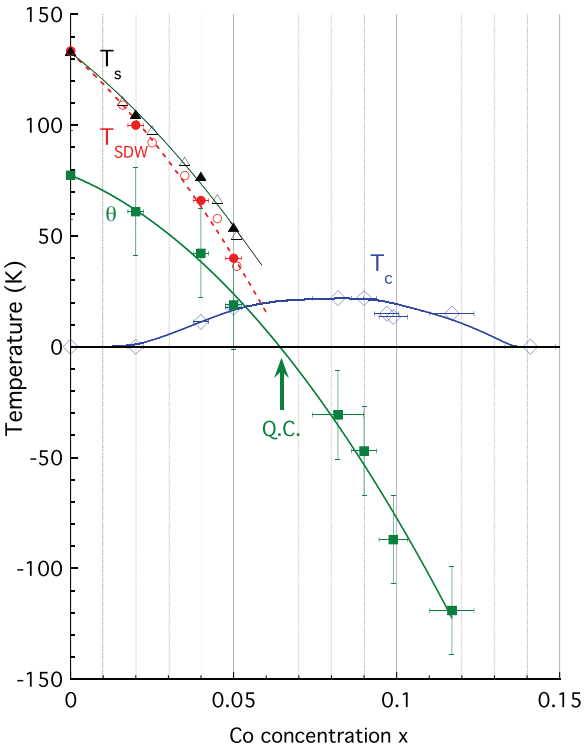

FIG. 1. (Color online) The superconducting transition temperature T_c of the present series of samples (◇) [10,26]; the tetragonal to orthorhombic structural phase transition temperature T_s determined from the onset of the NMR line broadening (▲); the SDW transition temperature $T_{\rm SDW}$ determined from the power-law fit of $1/T_1$ in the critical region (●); and Weiss temperature θ of the imaginary part of the staggered spin susceptibility $\chi''(\mathbf{q},\omega_n)$ determined by the mean-field fit of the $1/T_1T$ in the tetragonal phase (■) [26]. For comparison, we also show T_s (△) and $T_{\rm SDW}$ (○) as determined by anomalies observed in resistivity [11]. Upward arrow marks the magnetic quantum critical point $x_c \sim 0.065$ [26]. All solid lines are guides for the eye.

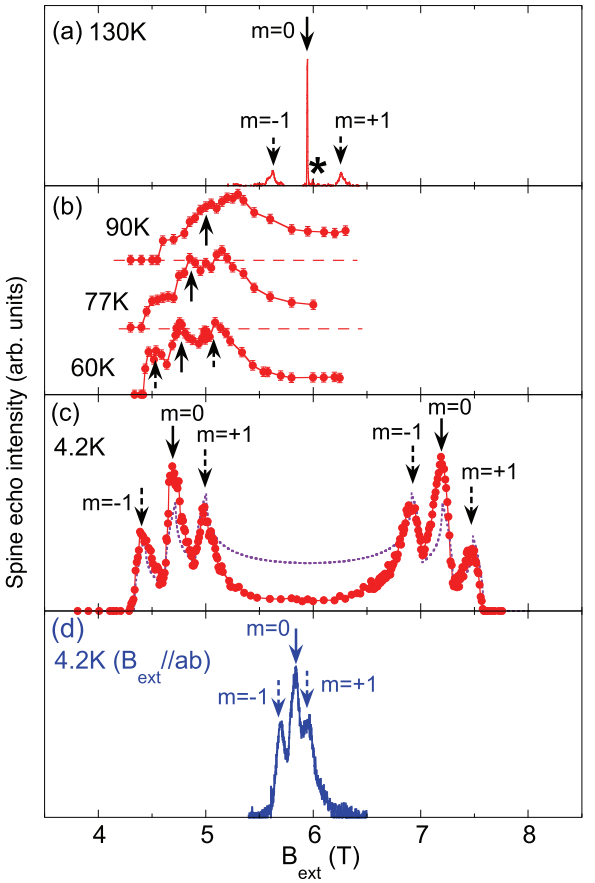

FIG. 2. (Color online) (a)–(c) Field-swept NMR line shapes of $Ba(Fe_{0.98}Co_{0.02})_2As_2$ obtained for a fixed frequency of 43.503 MHz under the external magnetic $B_{\rm ext}$ applied along the c axis. Solid and dashed arrows represent the central ($m = 0$) and satellite ($m = \pm 1$) transitions. The "star" in (a) marks a weak $m = 0$ peak arising from ^{75}As(1) sites located at the nearest neighbor of Co sites (see [26] for details). The vertical origin for the data points at 77 and 90 K is shifted for clarity. The dotted curve in (c) represents an attempt to fit the line shape at 4.2 K with a sinusoidally modulated static hyperfine field expected for an incommensurate SDW. (d) The line shape obtained for $B_{\rm ext} \parallel ab$.

we could resolve the fine structures of the NMR line shapes in the magnetically ordered state below $T_{\rm SDW}$ [see Figs. 2(b) and 2(c)], which we were unable to detect in our earlier study using a larger, inhomogeneous crystal [22]. Due to the poor signal-to-noise ratio arising from the small volume of the crystal and long relaxation time T_1, the NMR data acquisition is extremely time consuming below $T_{\rm SDW}$; it took up to ∼10 days of continuous signal averaging to complete one set of NMR line-shape measurements at a given temperature.

Small single-crystal samples used for other compositions with $x = 0.04$ and 0.05 are identical with those used in our previous studies [10,26]. We found stretched forms of T_1 recovery only for $x = 0.05$ below ∼70 K, analogous to the earlier report [24]. It is worth recalling that Co substitution is known to suppress spin fluctuations *locally* at Co sites, as evidenced by temperature independent $1/T_1T$ observed at Co sites at low temperatures [27]. A level of distribution in the electronic properties in the alloyed samples of $Ba(Fe_{1-x}Co_x)_2As_2$ is therefore naturally expected, as we demonstrated earlier from the variation of $1/T_1$ within a single NMR peak of a given composition [10]. But, none of the key findings and conclusions in this work rely on the $x = 0.05$ sample at low temperatures, and hence the issue of the inhomogeneity induced by Co substitution is beyond the scope of this work.

III. RESULTS AND DISCUSSIONS

A. ^{75}As NMR line shape, width, and Knight shift

In Fig. 2(a), we present a representative field-swept ^{75}As NMR line shape of $Ba(Fe_{0.98}Co_{0.02})_2As_2$ observed at a fixed NMR frequency of $\omega_n/2\pi = 43.503$ MHz in the paramagnetic state above $T_{\rm SDW}$. In general, the nuclear spin Hamiltonian can be expressed as a summation of the Zeeman and nuclear quadrupole interaction terms

$$H = -\gamma_n h\vec{B}\cdot\vec{I} + \frac{h\nu_Q^c}{6}\left\{3I_z^2 - I(I+1) + \frac{1}{2}\eta(I_+^2 + I_-^2)\right\}, \quad (1)$$

where the ^{75}As nuclear gyromagnetic ratio is $\gamma_n/2\pi = 7.2919$ MHz/T, h is Planck's constant, and $\vec{I}$ represents the nuclear spin. Since ^{75}As has nuclear spin $I = \frac{3}{2}$, we observe three transitions from $I_z = \frac{2m-1}{2}$ to $\frac{2m+1}{2}$ (with $m = -1, 0$, and $+1$) in the NMR line shape: the sharp central peak arises from the $I_z = -\frac{1}{2}$ to $+\frac{1}{2}$ transition ($m = 0$); additionally, two broad satellite peaks arise from $I_z = \pm\frac{3}{2}$ to $\pm\frac{1}{2}$ transitions ($m = \pm 1$), separated by $^{75}\nu_Q^c$. The nuclear quadrupole interaction frequency ν_Q^c along the c axis is proportional to the electric field gradient (EFG) at the observed ^{75}As site, and η is the asymmetry parameter of the EFG, $\eta = |\nu_Q^a - \nu_Q^b|/\nu_Q^c$. Due to the tetragonal symmetry at the ^{75}As sites, $\eta = 0$ above T_s. Co doping induces substantial disorder in the lattice, reflected on the distribution of $^{75}\nu_Q^c$.

$\vec{B}$ is the summation of the external field $\vec{B}_{\rm ext}$ and the time-averaged hyperfine fields from nearby electron spins $\vec{B}_{hf}$, i.e., $\vec{B} = \vec{B}_{\rm ext} + \vec{B}_{hf}$. In the paramagnetic state, the central peak frequency is slightly shifted (i.e., "Knight shift") due to small hyperfine fields induced by polarized electron spins nearby. Since the spin polarization induced by $\vec{B}_{\rm ext}$ is proportional to spin susceptibility $\chi_{\rm spin}$, we can measure the latter by accurately determining the central peak position [28]. In the SDW ordered state, static $\vec{B}_{hf}$ induced by ordered magnetic moments in the vicinity of the observed ^{75}As nuclear spins dramatically affects the NMR line shapes, as shown in Figs. 2(b) and 2(c). We will come back to this point below in Sec. III C.

We summarize the temperature dependence of the paramagnetic NMR Knight shift ^{75}K and the FWHM (full width at half maximum) of the central peak frequency in Figs. 3 and 4, respectively. To ensure high accuracy, we conducted these measurements by taking the FFT (fast Fourier transform) of the spin-echo envelope in a fixed magnetic field. The NMR Knight shift $^{75}K = A_{hf}\chi_{\rm spin} + K_{\rm chem}$ probes the local spin

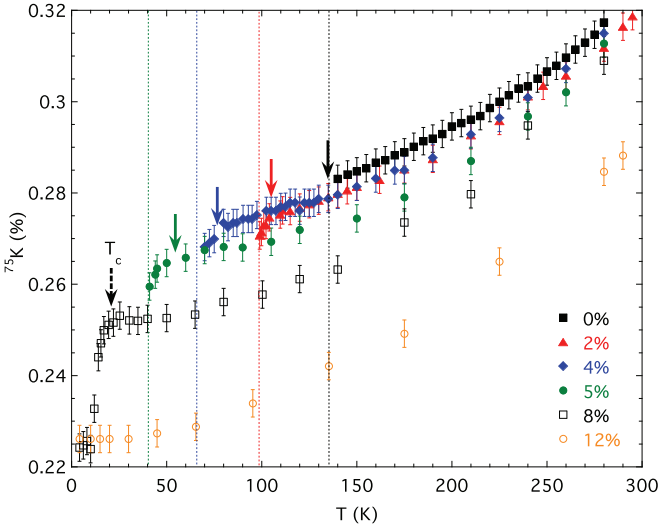

FIG. 3. (Color online) The ^{75}As NMR Knight shift ^{75}K observed in $B_{\rm ext} \parallel c$ for $Ba(Fe_{0.98}Co_{0.02})_2As_2$ is compared with the case of $x = 0$, 0.04, 0.05, 0.08, and 0.12 [10,26,27]. Downward solid arrows mark T_s, while vertical dotted line represents $T_{\rm SDW}$ as determined by the divergence of $1/T_1$. Notice the downturn of ^{75}K below T_s for $x = 0.02$, 0.04, and 0.05.

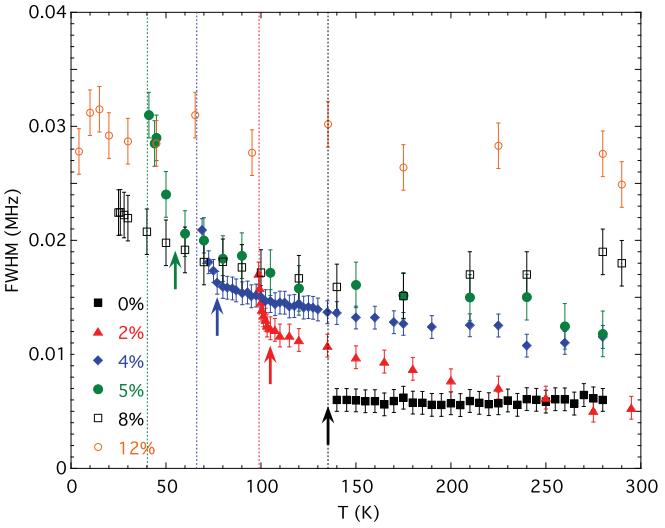

FIG. 4. (Color online) FWHM of the ^{75}As NMR central transition in an external magnetic field of $B_{\rm ext} \simeq 8.3$ T applied along the crystal c axis. Upward solid arrows mark T_s, while vertical dotted line represents $T_{\rm SDW}$. Notice the sudden upturn of FWHM below T_s for $x = 0.02$, 0.04, and 0.05. The plot of FWHM data is discontinued at $T_{\rm SDW}$ because NMR lines split below $T_{\rm SDW}$, as shown in Figs. 2(b) and 2(c).

susceptibility $\chi_{\rm spin}$ via hyperfine coupling A_{hf}; $K_{\rm chem}$ (~0.2 % or less for $x = 0.02$) is a temperature-independent chemical shift [27]. Our new results of ^{75}K in $Ba(Fe_{0.98}Co_{0.02})_2As_2$ are analogous to those observed for other compositions [10,26,27]: ^{75}K decreases with temperature, and tends to level off near ~100 K [29]. See [26] for detailed analysis of ^{75}K based on fitting the data with a pseudogap $\Delta_{PG}/k_B \sim 450$ K.

One interesting aspect of Fig. 3 is that ^{75}K exhibits a noticeable drop below 105.0 ± 0.5 K for $Ba(Fe_{0.98}Co_{0.02})_2As_2$. This anomaly is accompanied by a sudden onset of the divergent behavior of FWHM, as shown in Fig. 3. We note that FWHM indeed diverges below $T_{\rm SDW} = 99.0 \pm 0.5$ K, where the emergence of static hyperfine magnetic field B_{hf} splits the NMR line in the SDW ordered state, as shown in Figs. 2(b) and 2(c). We found analogous anomalies of ^{75}K and FWHM for Co 4% and 5% doped samples at 77 ± 2 K and 55 ± 2 K, respectively, as shown in Figs. 3 and 4. We summarize the concentration dependence of these anomalies in Fig. 1. Clearly, these anomalies are related to the structural phase transition at T_s [11,12].

Having identified the signature of the structural phase transition at T_s in our NMR data for the central transition, we also searched for an anomaly in the nuclear quadrupole frequency $^{75}\nu_Q^c$ by measuring the splitting between the central and satellite peaks. We recall that, in typical second-order structural phase transitions such as the high-temperature tetragonal to low-temperature orthorhombic phase transition in the undoped and Sr-doped La_2CuO_4 high-T_c cuprates, one could even observe a λ-like kink in the temperature dependence of ν_Q^c [30]. We summarize our results for $Ba(Fe_{0.98}Co_{0.02})_2As_2$ in Fig. 5. (High-precision determination of $^{75}\nu_Q^c$ is rather difficult for higher Co concentrations because the satellite peaks become very broad due to disorder [27].) In the case of undoped $BaFe_2As_2$, $^{75}\nu_Q^c$ exhibits a step at the first-order structural

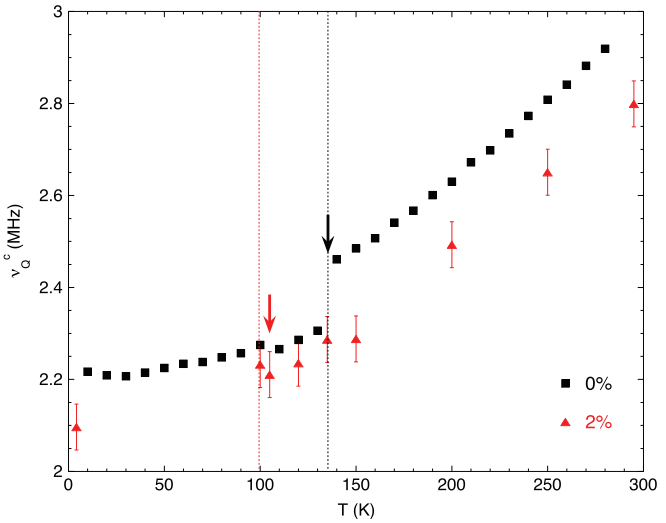

FIG. 5. (Color online) The c-axis component of the ^{75}As nuclear quadrupole frequency $^{75}\nu_Q^c$ in (▲) $Ba(Fe_{0.98}Co_{0.02})_2As_2$ (this work), and (■) undoped $BaFe_2As_2$ [8]. Downward arrows mark T_s, while vertical dotted line represents T_{SDW}. We were unable to determine $^{75}\nu_Q^c$ accurately below $T_{SDW} = 99.0$ K except at 4.2 K due to extremely broad line profiles [see Fig. 2(b)].

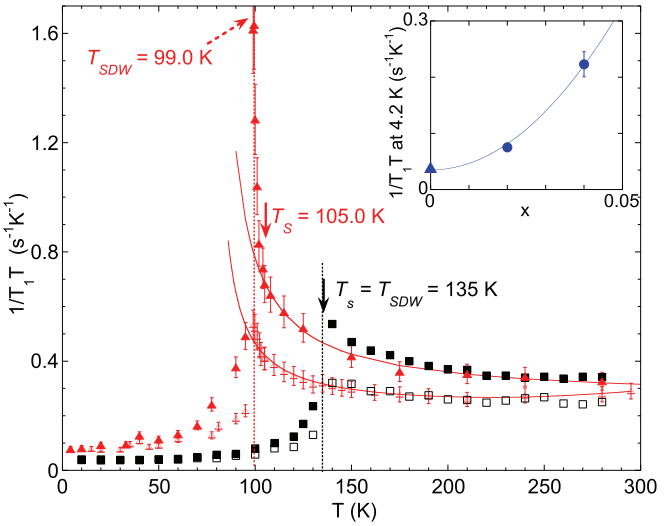

FIG. 6. (Color online) $1/T_1T$ observed for $Ba(Fe_{0.98}Co_{0.02})_2As_2$ under the external magnetic field $B_{ext} \parallel ab$ (▲) or $B_{ext} \parallel c$ (△). For comparison, we also show the results of $BaFe_2As_2$ for $B_{ext} \parallel ab$ (■) and $B_{ext} \parallel c$ (□) [8]. Vertical dotted lines represent T_{SDW}, while solid arrows mark T_s. Solid curves are a Curie-Weiss fit (see main text). Notice that the Curie-Weiss fit breaks down at $T_s = 105.0$ K, and $1/T_1T$ begins to blow up toward $T_{SDW} = 99.0$ K. Inset: the concentration x dependence of $1/T_1T$ at 4.2 K for $B_{ext} \parallel c$. The solid curve is a parabolic fit.

transition $T_s = 135$ K [8], but we find practically no anomaly at $T_s = 105.0$ K for the Co 2% sample. In general, when the lattice contracts with decreasing temperature, the lattice contribution to the electric field gradient (EFG), and hence to ν_Q, increases. Our finding that $^{75}\nu_Q^c$ smoothly decreases with temperature might be an indication that there is a sizable onsite ionic contribution with an opposite sign.

It is not clear why $^{75}\nu_Q^c$ does not exhibit a clear anomaly at T_s for the Co 2% doped sample. One possible scenario is that the influence of structural distortion on ^{75}As sites becomes so subtle under the presence of Co dopants that the change of $^{75}\nu_Q^c$ also becomes extremely small. We also recall that softening of the lattice stiffness begins at unusually high temperatures in $Ba(Fe_{1-x}Co_x)_2As_2$, and has been speculated to be the consequence of antiferromagnetic correlations [31–33]. Perhaps the effects of orthorhombic distortion on $^{75}\nu_Q^c$ appear progressively from much higher temperature than T_s. In any event, the absence of a strong signature of structural anomaly in the temperature dependence of $^{75}\nu_Q^c$ at T_s excludes the possibility that anomalies observed below T_s in Figs. 3 and 4 are a consequence of the subtle changes in the second-order quadrupole effects. In fact, we confirmed that the FWHM is approximately proportional to the magnitude of the applied magnetic field, hence the divergent behavior of FWHM below T_s is the consequence of magnetic effects. We recall that the NMR line broadened by the second-order quadrupole effects would be inversely proportional to the magnetic field instead.

Quite generally, divergence of the NMR linewidth precedes a magnetic phase transition through the divergence of dynamical spin susceptibility in the critical regime [28]. We also recall that the NMR Knight shift ^{75}K reflects local paramagnetic spin susceptibility χ_{spin}, hence, the downturn in the temperature dependence of ^{75}K below T_s is also consistent with suppression of χ_{spin} due to strong antiferromagnetic short-range order. Thus, our findings in both Figs. 3 and 4 suggest that the structural phase transition at T_s drives the onset of strong 3D antiferromagnetic short-range order. This point is more vividly demonstrated through the divergent behavior of $1/T_1$ in the next section.

B. Critical spin dynamics near T_{SDW}

In Fig. 6, we present ^{75}As nuclear spin-lattice relaxation rate $1/T_1$ divided by temperature T, i.e., $1/T_1T$, observed for $Ba(Fe_{0.98}Co_{0.02})_2As_2$. $1/T_1T$ measures wave-vector $\mathbf{q}$ integral of the imaginary part of the dynamical electron spin susceptibility $\chi''(\mathbf{q},\omega_n)$ weighted by the hyperfine form factor $|A_{hf}(\mathbf{q})|^2$ [34]. In the case of undoped $BaFe_2As_2$, $1/T_1T$ does not show divergent behavior at T_{SDW} expected for second-order magnetic phase transitions; instead, $1/T_1T$ shows a step at 135 K because the SDW transition is first order [8]. In contrast, $1/T_1T$ observed for Co 2% doped sample exhibits strongly divergent behavior near T_{SDW} in the geometry of $B_{ext} \parallel ab$. In this configuration, $1/T_1T$ probes fluctuations of hyperfine fields both along the c axis and ab plane. The divergent signature is less prominent for $B_{ext} \parallel c$ because $1/T_1T$ probes fluctuating hyperfine fields only within the ab plane, and the transferred hyperfine field $A_{hf}(\mathbf{q})$ becomes vanishingly small for staggered wave vectors in this configuration [8,15,34]. In other words, it is advantageous to use the $B_{ext} \parallel ab$ geometry to probe the critical behavior of the SDW transition.

Accordingly, in what follows, we focus our attention on $1/T_1T$ measured in $B_{ext} \parallel ab$. In Fig. 7, we show $1/T_1T$ in a semi-log scale for various Co concentrations. To avoid confusion, we show only the results above T_{SDW} (for $x \leqslant 5\%$) or T_c (for $x = 8\%$ and 12%). Also presented is a phenomenological Curie-Weiss fit to an empirical equation

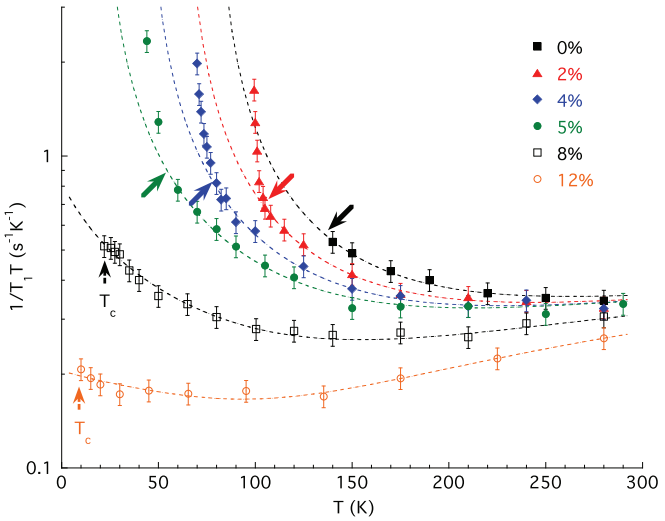

FIG. 7. (Color online) A semi-log plot of $1/T_1T$ observed for $Ba(Fe_{1-x}Co_x)_2As_2$ with $B_{ext} \parallel ab$. For clarity, we show data points only above T_{SDW} for $x \leqslant 0.05$, and above T_c for $x = 0.08$ and 0.12. Dashed curves represent a phenomenological Curie-Weiss fit, incorporating a background term due to a pseudogap (see main text). Slanted solid arrows mark T_s for $x = 0\% \sim 5\%$, while vertical dashed arrows show T_c for $x = 8\%$ and 12%.

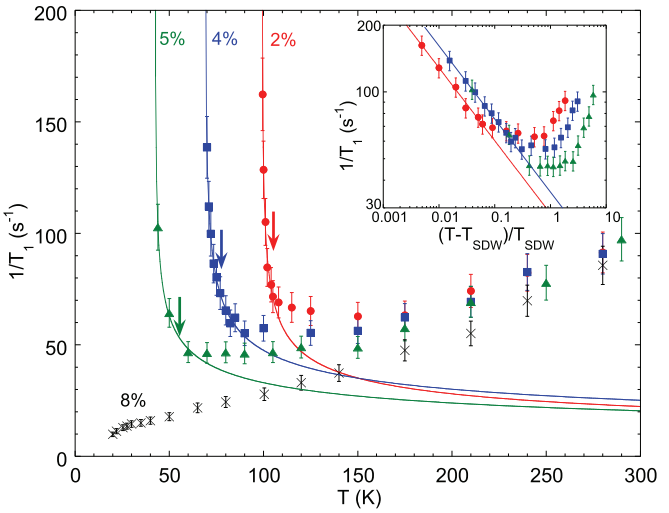

FIG. 8. (Color online) Power-law fits of $1/T_1$ in the critical region of underdoped $Ba(Fe_{1-x}Co_x)_2As_2$. Dotted curve and solid arrows mark T_s and T_{SDW}, respectively. Inset: log-log plot of $1/T_1$ as a function of the reduced temperature $(T/T_{SDW} - 1)$. Solid lines represent a power-law behavior in the critical region with $\delta = 0.33$.

$1/T_1T = C/(T - \theta) + A\exp(-\Delta_{PG}/k_BT)$ [26]. C and A are fitting parameters, and θ is the Weiss temperature of the staggered spin susceptibility $\chi''(\mathbf{q},\omega_n)$ near the ordering vector. The concentration dependence of θ thus obtained is summarized in Fig. 1. Note that we have reversed the sign convention for θ in the present work (i.e., $-\theta$ in Fig. 1 corresponds to $+\theta$ in [26]). The second, activation term in the fit represents the background contributions which decrease with temperature, reflecting the pseudogaplike signature commonly observed for iron-pnictide and iron-selenide superconductors [26,35–39]. As already discussed in detail in [26], the phenomenological Curie-Weiss fit captures the temperature and concentration dependence of $\chi''(\mathbf{q},\omega_n)$ remarkably well, including the new results for the Co 2% doped sample. The Curie-Weiss behavior of $1/T_1T$ reflects the fact that, upon cooling, short-range antiferromagnetic correlations slowly grow toward T_{SDW}. θ reverses its sign above the quantum critical point $x_c \sim 0.065$, which implies that Fe spins are not destined to order above x_c. Remarkably, the optimally superconducting composition with the maximum $T_c \sim 25$ K is located in the vicinity of x_c, hinting at the link between the superconducting mechanism and spin fluctuations [26].

Another important feature of Figs. 6 and 7 which we did not discuss explicitly in [26] is that the phenomenological Curie-Weiss fit breaks down below T_s. Extrapolation of the fit to below T_s underestimates the data points near the SDW phase transition for Co 2%, 4%, and 5%, and strong divergent behavior sets in at T_s. In other words, the three-dimensional short-range order sets in at the tetragonal to orthorhombic structural phase transition, which is prerequisite to the critical slowing down of spin fluctuations toward the eventual three-dimensional SDW order. Analogous interplay between the spin and lattice degrees of freedom was also observed for LaFeAsO [40].

In Fig. 8, we plot $1/T_1$ of three underdoped compositions on a linear scale. We note that $1/T_1 \propto \Sigma_{\mathbf{q}}|A_{hf}(\mathbf{q})|^2S(\mathbf{q},\omega_n)$, where $S(\mathbf{q},\omega_n)$ is the dynamical structure factor. $1/T_1$ is a very convenient probe to study the critical dynamics of $S(\mathbf{q},\omega_n)$ in the immediate vicinity of magnetic phase transitions because (i) one can probe the dynamics at extremely low energy ($\hbar\omega_n \sim \mu$ eV), and (ii) the wave-vector integral is automatically done. Below T_s, we can fit the critical dynamics with a power-law $1/T_1 \propto (T/T_{SDW} - 1)^{-\delta}$. We determined T_{SDW} and the critical exponent δ based on the best fit. The resultant values of $T_{SDW} = 99.0$ K (Co 2 %), 68.9 K (Co 4 %), and 42.3 K (Co 5%) are summarized in Fig. 1. The best fit also resulted in the critical exponent $\delta = 0.329$ for Co 2 %, and 0.317 for Co 4%. The aforementioned distribution of $1/T_1$ below ~70 K for Co 5% makes it difficult to estimate δ with high accuracy, but the observed temperature dependence is consistent with $\delta \simeq 0.33$. The inset of Fig. 8 shows a log-log plot of $1/T_1$ as a function of the reduced temperature $(T/T_{SDW} - 1)$. The common slope in the vicinity of the SDW transition indicates that the SDW transition of all three compositions belongs to the same universality class, and the critical exponent is given by $\delta \sim 0.33$. This value is close to $\delta = 0.33 \pm 0.01$ observed for a Mott-insulator CuO [17] in the vicinity of the Néel transition at $T_N = 229$ K, and consistent with the prediction for insulating three-dimensional Heisenberg antiferromagnets $\delta \sim 0.35$ [18–21].

C. Ordered moments

In Figs. 2(b) and 2(c), we show the effects of SDW ordering on the field-swept NMR line shapes of $Ba(Fe_{0.98}Co_{0.02})_2As_2$ with $B_{ext} \parallel c$. We confirmed the symmetrical nature of the line shape at 4.2 K, as expected, hence only the lower field half of the line shapes was measured in the intermediate temperature range between 4.2 K and T_{SDW}. Below T_{SDW}, the entire ^{75}As NMR line shape begins to split. As noted first by Kitagawa *et al.* in the case of undoped $BaFe_2As_2$ [8], this is because the

static hyperfine magnetic field B_{hf} at ^{75}As sites arising from the ordered Fe moments within the Fe layers points toward the $+c$ or $-c$ axis. For this reason, the overall NMR line shape shifts only slightly without exhibiting a splitting under the configuration of $B_{\rm ext} \parallel ab$, as shown in Fig. 2(d).

While the observed NMR line shapes below $T_{\rm SDW}$ bear similarities with the case of undoped $BaFe_2As_2$, there is one major difference [22]: our NMR line shapes in Figs. 2(b) and 2(c) exhibit a continuum in the middle. The integrated intensity between $B_{\rm ext} = 5.474$ to 6.475 T accounts for ~8.5% of the overall intensity. This implies that ~8.5% of ^{75}As nuclear spins experience $|B_{hf}| \leqslant 0.5$ T, while the maximum value of the hyperfine field reaches $B_{hf}^{\rm max} = 1.27$ T at 4.2 K. Our attempt to fit the observed line shape with one-dimensional incommensurate modulation $B_{hf} = B_{hf}^{\rm max}\sin(\vec{q}\cdot\vec{x})$, where $\vec{q}$ represents the incommensurate SDW ordering vector, is unsatisfactory, as shown in Fig. 2(c). Notice that the calculated results grossly overestimate the spectral weight in the middle part of the line shape. In view of the fact that the integrated intensity of the ^{75}As(1) sites with a Co atom in one of their four nearest-neighbor Fe sites also accounts for approximately ~7.5% of the intensity [see asterisk in Fig. 2(a)] [26], the continuum in the middle part of the NMR line shape may arise primarily from ^{75}As(1) sites. That is, Co dopants may be suppressing the Fe magnetic moments locally. It has been shown by neutron scattering that the SDW is commensurate with the lattice up to $x = 0.056$ [42,43]. Based on our NMR data, we can not prove or disprove the incommensurability at $x = 0.02$. We note that similar ^{75}As line shapes have been observed in the lightly doped regime of $Ba(Fe_{1-x}Ni_x)_2As_2$ ($x =$ 0.0072 and 0.016) [24].

We summarize the temperature dependence of $B_{hf}^{\rm max}$ in Fig. 9. $B_{hf}^{\rm max}$ remains approximately constant up to ~30 K, then decreases continuously toward $T_{\rm SDW} = 99.0$ K. This behavior

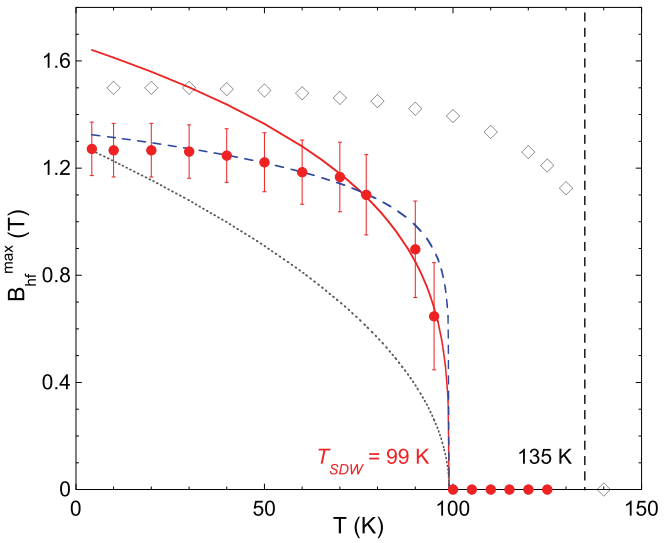

FIG. 9. (Color online) The temperature dependence of $B_{hf}^{\rm max}$ for $Ba(Fe_{0.98}Co_{0.02})_2As_2$ (●). For comparison, we also show B_{hf}^{c} reported for $BaFe_2As_2$ (◇) in [8]. The solid line shows $B_{hf} \sim (99.0 - T)^{\beta}$ with a critical exponent $\beta = 0.30$. The dotted and dashed lines are for $\beta = 0.5$ and 0.125 plotted by fixing at two ends ($T = 0$ and 99.0 K), respectively.

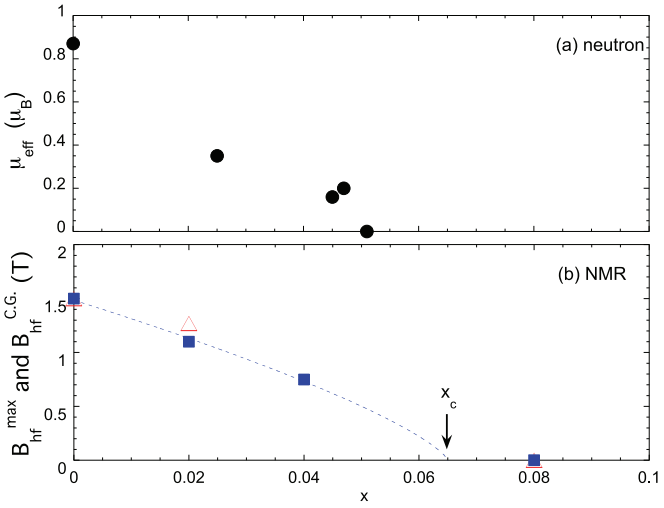

FIG. 10. (Color online) (a) (●): The concentration x dependence of the magnitude of the ordered moment $\mu_{\rm eff}$ for $Ba(Fe_{1-x}Co_x)_2As_2$ as determined by neutron diffraction measurements [6,41,42]. (b) The maximum $B_{hf}^{\rm max}$ (△) and center of gravity $B_{hf}^{C.G.}$ (■) of the distribution of the hyperfine field. The NMR result for $x = 0$ is from [8], while $x_c \sim 0.065$ was determined from the Curie-Weiss fit of the $1/T_1T$ data [26] (see Fig. 1). The dotted curve is a guide for eyes.

is markedly different from the first-order commensurate SDW transition in $BaFe_2As_2$ [8]; B_{hf} decreases discontinuously at $T_{\rm SDW} = 135$ K in the latter. By fitting the temperature dependence of $B_{hf}^{\rm max}$ between 70 K (~$0.7T_{\rm SDW}$) and $T_{\rm SDW} =$ 99.0 K to a power law, $B_{hf}^{\rm max} \sim (T_{\rm SDW} - T)^{\beta}$ with a fixed $T_{\rm SDW} = 99.0$ K, we obtain the critical exponent $\beta \sim 0.3$. Very broad line shapes make accurate determination of $B_{hf}^{\rm max}$ difficult near $T_{\rm SDW}$, hence we were unable to eliminate the large uncertainties of β. Nonetheless, it is worth pointing out that $\beta \sim 0.3$ is consistent with the expectation from the Heisenberg model $\beta = 0.37$, but different from the mean-field value $\beta = 0.5$.

Turning our attention to the magnitude of the ordered moment $\mu_{\rm eff}$ at 4.2 K as a function of x, we compare NMR results with those obtained from neutron scattering in Fig. 10. Since B_{hf} has a distribution under the presence of Co dopants, we plot both the maximum value and the center of gravity of the hyperfine field $B_{hf}^{\rm max}$ and $B_{hf}^{C.G.}$, respectively, in Fig. 10(b). We recall that $\mu_{\rm eff} = 0.87\mu_B$ at 4.2 K for the parent compound $BaFe_2As_2$ [6], and Co doping suppresses $\mu_{\rm eff}$ [41,42], as summarized in Fig. 10(a). On the other hand, $B_{hf}^{\rm max} = B_{hf}^{C.G.} =$ 1.5 T observed earlier for $BaFe_2As_2$ [8] is gradually suppressed by Co doping. Our results of B_{hf} smoothly extrapolate to the critical concentration as determined from the analysis of $1/T_1T$ in Fig. 1, $x_c \sim 6.5\%$.

D. Low-energy spin excitations below $T_{\rm SDW}$

In Fig. 6, we show the temperature dependence of $1/T_1T$ below $T_{\rm SDW}$. Our results show a typical λ-like temperature dependence in the vicinity of the SDW transition. In insulating antiferromagnets, the low-temperature behavior of $1/T_1T$ is usually dominated by multimagnon Raman processes, and $1/T_1T$ decreases very quickly [28]. In the present case,

however, as we approach the base temperature of 4.2 K, $1/T_1T$ levels off to a constant value of $1/T_1T \sim 0.08\ (s^{-1}K^{-1})$. Analogous behavior was previously reported also for the undoped parent phase $BaFe_2As_2$, and was attributed to the Korringa process arising from low-energy electron-hole pair excitations at the reconstructed Fermi surface [8]. We summarize the values of $1/T_1T$ observed at 4.2 K as a function of the doping content x in the inset of Fig. 6, including our preliminary results for $x = 0.04$ [22]. Interestingly, three data points fit nicely with a parabolic function of x. If the sizable magnitude of $1/T_1T$ at 4.2 K indeed arises from the Korringa process, we expect $1/T_1T \propto D(E_F)^2$, where $D(E_F)$ is the density of states. That is, the observed parabolic increase of $1/T_1T$ implies that $D(E_F)$ increases roughly linearly with x. We note that if we apply a simple rigid band picture to the reconstructed Fermi surfaces, simple dimensional analysis of E_F and $D(E_F)$ in three dimensions would lead to $D(E_F) \propto x^{1/3}$ instead, where x is the number of conduction electrons.

IV. SUMMARY AND CONCLUSIONS

We have presented an in-depth ^{75}As NMR study of the critical behavior of the SDW transition in the lightly Co-doped regime of $Ba(Fe_{1-x}Co_x)_2As_2$, with the primary focus on $x = 0.02$. We identified the NMR signatures of the tetragonal to orthorhombic structural phase transition preceding the SDW transition. Our Knight shift, NMR linewidth, and $1/T_1$ data suggest that the strong short-range SDW order with three-dimensional nature sets in once the FeAs planes lower the symmetry from tetragonal to orthorhombic. In the orthorhombic phase below T_s, simplistic fits of the antiferromagnetic contribution to $1/T_1T$ based on a Curie-Weiss law using two free parameters (Fig. 7) or 2D SCR (self-consistent renormalization) theory with four free parameters [44] fail to capture the critical behavior. Precisely at T_s, critical slowing down of spin fluctuations sets in, and the critical exponent for the divergence of the dynamical structure factor $S(\mathbf{q},\omega_n)$ is $\delta \sim 0.33$, as generally expected for insulating 3D Heisenberg antiferromagnets. Our fitting range is rather limited and it is difficult to draw a definitive conclusion, but this value is inconsistent with $\delta = 0.5$ expected for the 3D SCR theory for itinerant antiferromagnets [45].

ACKNOWLEDGMENTS

The work at Zhejiang was supported by National Basic Research Program of China (Grants No. 2014CB921203 and No. 2011CBA00103), NSF of China (Grant No. 11274268). The work at McMaster was supported by NSERC and CIFAR. The work at Oak Ridge National Laboratory was supported by the Department of Energy, Basic Energy Sciences, Materials Sciences and Engineering Division. The work at Beijing and Nanjing was supported by NSFC, the Ministry of Science and Technology of China, and the Chinese Academy of Sciences.

[1] X. H. Chen, T. Wu, G. Wu, R. H. Liu, H. Chen, and D. F. Fang, Nature (London) **453**, 761 (2008).
[2] Y. Kamihara, T. Watanabe, M. Hirano, and H. Hosono, J. Am. Chem. Soc. **130**, 3296 (2008).
[3] Z. A. Ren, W. Lu, J. Yang, W. Yi, X. L. Shen, Z. C. Li, G. C. Che, X. L. Dong, L. L. Sun, F. Zhou, and Z. X. Zhao, Chin. Phys. Lett. **25**, 2215 (2008).
[4] M. Rotter, M. Tegel, and D. Johrendt, Phys. Rev. Lett. **101**, 107006 (2008).
[5] A. S. Sefat, R. Jin, M. A. McGuire, B. C. Sales, D. J. Singh, and D. Mandrus, Phys. Rev. Lett. **101**, 117004 (2008).
[6] Q. Huang, Y. Qiu, W. Bao, M. A. Green, J. W. Lynn, Y. C. Gasparovic, T. Wu, G. Wu, and X. H. Chen, Phys. Rev. Lett. **101**, 257003 (2008).
[7] H. Fukazawa, K. Hirayama, K. Kondo, T. Yamazaki, Y. Kohori, N. Takeshita, K. Miyazawa, H. Kito, H. Eisaki, and A. Iyo, J. Phys. Soc. Jpn. **77**, 093706 (2008).
[8] K. Kitagawa, N. Katayama, K. Ohgushi, M. Yoshida, and M. Takigawa, J. Phys. Soc. Jpn. **77**, 114709 (2008).
[9] N. Ni, M. E. Tillman, J. Q. Yan, A. Kracher, S. T. Hannahs, S. L. Bud'ko, and P. C. Canfield, Phys. Rev. B **78**, 214515 (2008).
[10] F. L. Ning, K. Ahilan, T. Imai, A. S. Sefat, R. Jin, M. A. McGuire, B. C. Sales, and D. Mandrus, J. Phys. Soc. Jpn. **78**, 013711 (2009).
[11] J. H. Chu, J. G. Analytis, C. Kucharczyk, and I. R. Fisher, Phys. Rev. B **79**, 014506 (2009).
[12] S. Nandi, M. G. Kim, A. Kreyssig, R. M. Fernandes, D. K. Pratt, A. Thaler, N. Ni, S. L. Bud'ko, P. C. Canfield, J. Schmalian, R. J. McQueeney, and A. I. Goldman, Phys. Rev. Lett. **104**, 057006 (2010).
[13] X. F. Wang, T. Wu, J. Wu, R. H. Liu, X. H. Chen, and Y. L. Xie, New J. Phys. **11**, 045003 (2009).
[14] L. Fang, H. Luo, P. Cheng, Z. Wang, Y. Jia, G. Mu, B. Shen, I. I. Mazin, L. Shan, C. Ren, and H.-H. Wen, Phys. Rev. B **80**, 140508(R) (2009).
[15] D. C. Johnston, Adv. Phys. **59**, 803 (2010).
[16] K. Kontani and Y. Masuda, J. Magn. Magn. Mater. **31-34**, 287 (1993).
[17] Y. Itoh, T. Imai, T. Shimizu, T. Tsuda, H. Yasuoka, and Y. Ueda, J. Phys. Soc. Jpn. **59**, 1143 (1990).
[18] B. I. Halperin and P. C. Hohenberg, Phys. Rev. Lett. **19**, 700 (1967).
[19] C. Hohenemser, N. Rosov, and A. Kleinhammes, Hyperfine Interact. **49**, 267 (1989).
[20] K. Kawasaki, Prog. Theor. Phys. **39**, 285 (1968).
[21] S. W. Lovesey, E. Balcar, and A. Cuccoli, J. Phys.: Condens. Matter **7**, 2615 (1995).
[22] F. L. Ning, K. Ahilan, T. Imai, A. S. Sefat, R. Jin, M. A. McGuire, B. C. Sales, and D. Mandrus, Phys. Rev. B **79**, 140506(R) (2009).
[23] A. P. Dioguardi, J. Crocker, A. C. Shockley, C. H. Lin, K. R. Shirer, D. M. Nisson, M. M. Lawson, N. apRoberts-Warren, P. C. Canfield, S. L. Bud'ko, S. Ran, and N. J. Curro, Phys. Rev. Lett. **111**, 207201 (2013).
[24] A. P. Dioguardi, N. apRoberts-Warren, A. C. Shockley, S. L. Bud'ko, N. Ni, P. C. Canfield, and N. J. Curro, Phys. Rev. B **82**, 140411(R) (2010).

[25] F. Hammerath, U. Gräfe, T. Kühne, H. Kühne, P. L. Kuhns, A. P. Reyes, G. Lang, S. Wurmehl, B. Büchner, P. Carretta, and H.-J. Grafe, Phys. Rev. B **88**, 104503 (2013).
[26] F. L. Ning, K. Ahilan, T. Imai, A. S. Sefat, M. A. McGuire, B. C. Sales, D. Mandrus, P. Cheng, B. Shen, and H. H. Wen, Phys. Rev. Lett. **104**, 037001 (2010).
[27] F. L. Ning, K. Ahilan, T. Imai, A. S. Sefat, R. Jin, M. A. McGuire, B. C. Sales, and D. Mandrus, J. Phys. Soc. Jpn. **77**, 103705 (2008).
[28] V. Jaccarino, in *Proceedings of the International School of Physics, Enrico Fermi XXXVII* (Academic, New York, 1967).
[29] S. Oh, A. M. Mounce, S. Mukhopadhyay, W. P. Halperin, A. B. Vorontsov, S. L. Bud'ko, P. C. Canfield, Y. Furukawa, A. P. Reyes, and P. L. Kuhns, Phys. Rev. B **83**, 214501 (2011).
[30] T. Imai, C. P. Slichter, K. Yoshimura, and K. Kosuge, Phys. Rev. Lett. **70**, 1002 (1993).
[31] R. M. Fernandes, A. E. Böehmer, C. Meingast, and J. Schmalian, Phys. Rev. Lett. **111**, 137001 (2013).
[32] R. M. Fernandes, L. H. VanBebber, S. Bhattacharya, P. Chandra, V. Keppens, D. Mandrus, M. A. McGuire, B. C. Sales, A. S. Sefat, and J. Schmalian, Phys. Rev. Lett. **105**, 157003 (2010).
[33] M. Yoshizawa, D. Kimura, T. Chiba, A. Ismayil, Y. Nakanishi, K. Kihou, C. H. Lee, A. Iyo, H. Eisaki, M. Nakajima, and S. Uchida, J. Phys. Soc. Jpn. **81**, 024604 (2012).
[34] A. Smerald and N. Shannon, Phys. Rev. B **84**, 184437 (2011).
[35] K. Ahilan, F. L. Ning, T. Imai, A. S. Sefat, R. Jin, M. A. McGuire, B. C. Sales, and D. Mandrus, Phys. Rev. B **78**, 100501(R) (2008).
[36] T. Imai, K. Ahilan, F. L. Ning, T. M. McQueen, and R. J. Cava, Phys. Rev. Lett. **102**, 177005 (2009).
[37] D. A. Torchetti, M. Fu, D. C. Christensen, K. J. Nelson, T. Imai, H. C. Lei, and C. P. Petrovic, Phys. Rev. B **83**, 104508 (2011).
[38] Y. Nakai, K. Ishida, Y. Kamihara, M. Hirano, and H. Hosono, J. Phys. Soc. Jpn. **77**, 073701 (2008).
[39] R. Zhou, Z. Li, J. Yang, C. T. Lin, and G. Q. Zheng, Nat. Commun. **4**, 2265 (2013).
[40] M. Fu, D. A. Torchetti, T. Imai, F. L Ning, J.-Q. Yan, and A. S. Sefat, Phys. Rev. Lett. **109**, 247001 (2012).
[41] C. Lester, Jiun-Haw Chu, J. G. Analytis, S. C. Capelli, A. S. Erickson, C. L. Condron, M. F. Toney, I. R. Fisher, and S. M. Hayden, Phys. Rev. B **79**, 144523 (2009).
[42] D. K. Pratt, W. Tian, A. Kreyssig, J. L. Zarestky, S. Nandi, N. Ni, S. L. Bud'ko, P. C. Canfield, A. I. Goldman, and R. J. McQueeney, Phys. Rev. Lett. **103**, 087001 (2009).
[43] D. K. Pratt, M. G. Kim, A. Kreyssig, Y. B. Lee, G. S. Tucker, A. Thaler, W. Tian, J. L. Zarestky, S. L. Bud'ko, P. C. Canfield, B. N. Harmon, A. I. Goldman, and R. J. McQueeney, Phys. Rev. Lett. **106**, 257001 (2011).
[44] Y. Nakai, T. Iye, S. Kitagawa, K. Ishida, S. Kasahara, T. Shibauchi, Y. Matsuda, H. Ikeda, and T. Terashima, Phys. Rev. B **87**, 174507 (2013).
[45] T. Moriya, *Spin Fluctuations in Itinerant Electron Magnetism* (Springer, New York, 1985).